Journal of Molecular Medicine (2019) 97:691–709
https://doi.org/10.1007/s00109-019-01763-3

JMolMed

ORIGINAL ARTICLE

PRSS21/testisin inhibits ovarian tumor metastasis and antagonizes proangiogenic angiopoietins ANG2 and ANGPTL4

Gregory D. Conway[1] · Marguerite S. Buzza[1] · Erik W. Martin[1,2] · Nadire Duru[1] · Tierra A. Johnson[1] · Raymond J. Peroutka[1] · Nisha R. Pawar[1] · Toni M. Antalis[1]

Received: 30 October 2018 / Revised: 12 February 2019 / Accepted: 1 March 2019 / Published online: 25 March 2019

Abstract

Ovarian cancer is the leading cause of death among all the gynecological cancers in the USA. Ovarian cancer employs a unique mode of metastasis, as exfoliated tumor cells disseminate within the peritoneal cavity, colonizing in several sites as well as accumulating ascites. Tumor recurrence and widespread metastasis are significant factors contributing to poor prognosis. PRSS21 is a metastasis-associated ovarian cancer gene that encodes the glycosyl-phosphatidylinositol-linked serine protease, testisin. Testisin expression is increased in multiple ovarian tumor types, with relatively little expression in normal tissues, but is differentially decreased in metastatic ovarian serous carcinomas compared to primary tumors. Here we explored the function of testisin in late-stage ovarian cancer progression using a murine xenograft model of ovarian intraperitoneal tumor metastasis. Increased tumor testisin expression inhibited intra-peritoneal tumor seeding and colonization, ascites accumulation, and metastatic tumor burden that was dependent on catalytically active testisin. The known testisin substrate, protease-activated receptor-2 (PAR-2), is a target of testisin activity. Gene profiling and mechanistic studies demonstrate that testisin activity suppresses the synthesis and secretion of pro-angiogenic angiopoietins, ANG2 and ANGPTL4, which normally promote vascular leak and edema. These observations support a model wherein testisin activates PAR-2 to antagonize proangiogenic angiopoietins that modulate vascular permeability and ascites accumulation associated with ovarian tumor metastasis.

Key messages

- Testisin inhibits metastatic ovarian tumor burden and ascites production.
- Testisin activity antagonizes ANG2 and ANGPTL4 synthesis and secretion.
- PAR-2 is a proteolytic target of testisin on the surface of ovarian cancer cells.

Keywords Testisin · Ovarian metastasis · ANG2 · Ascites · Serine protease

Introduction

Ovarian cancer is the most lethal gynecological malignancy with a 5-year survival rate of only approximately 20% [1]. A majority of patients present with advanced disease, after the cancer has already locally metastasized throughout the peritoneal cavity when options for effective alternative treatments are limited. As a result, patients have a poor prognosis, which has seen only modest improvement in the past 30 years. There is clearly an urgent need to develop second-line therapies based on an understanding of alternative molecular mechanisms, to both improve the therapeutic efficacy of conventional treatments and to provide novel therapeutic options for patients with metastatic disease.

Electronic supplementary material The online version of this article (https://doi.org/10.1007/s00109-019-01763-3) contains supplementary material, which is available to authorized users.

✉ Toni M. Antalis
tantalis@som.umaryland.edu

[1] Center for Vascular and Inflammatory Diseases, Department of Physiology, and the University of Maryland Marlene and Stewart Greenebaum Comprehensive Cancer Center, University of Maryland School of Medicine, 800 West Baltimore Street Rm 220, Baltimore, MD 21201, USA

[2] Laboratory of Molecular Biology and Immunology, National Institute on Aging, NIH, Baltimore, MD, USA

Ovarian cancer originates in the ovary or fallopian tubes and, carried by peritoneal fluid, metastasizes directly into the peritoneal cavity, where the tumor cells seed the mesothelium of the omentum, diaphragm, bowel serosa, and the peritoneal walls [2]. Unlike breast, colon, or lung cancer, ovarian cancer rarely metastasizes by the hematogenous route [2]. A number of studies point to the remodeling of the vasculature and angiogenesis as important tumor microenvironmental mechanisms for ovarian cancer progression and metastasis [3, 4]. Ovarian tumors drive changes in vascular permeability, increasing peritoneal fluid accumulation, leading to the development of malignant ascites in two thirds of patients [5, 6]. The accumulation of ascites, rich in growth factors, cytokines, and proangiogenic factors further facilitates tumor cell proliferation and metastatic spread [5]. Studies show that malignant ascites production is associated with dysregulated endothelial barrier function of the peritoneal vasculature which leads to an increase in vascular permeability [6].

Testisin is a membrane-anchored serine protease that is frequently expressed in human epithelial ovarian cancers [7]. Previously identified by our laboratory, testisin is a serine protease attached to the cell surface via C-terminal glycosylphosphatidylinositol (GPI) anchor [8–11]. Testisin has a remarkably restricted normal tissue distribution, being expressed in abundance only in testis, where its genetic deletion in mice results in developmentally damaged spermatocytes [12]. While testisin expression is not detected in normal ovarian tissue or fallopian tubes [7, 10], testisin is upregulated in 80–90% of stage II and III ovarian tumors [7]. When ectopically expressed in human SKOV3 ovarian tumor cells, testisin was found to enhance colony formation in soft agar and to increase the size of subcutaneous xenografts in SCID mice [13]. However, testisin is also found to be downregulated in metastatic ovarian disease, when compared with primary ovarian carcinomas [14].

We have recently identified protease-activated receptor-2 (PAR-2) as a substrate of testisin [15]. PAR-2 belongs to a family of four seven-transmembrane G protein-coupled receptors that are activated by tethered ligands exposed by proteolytic removal of an amino-terminal exodomain [16]. Binding of the tethered ligand causes receptor activation and endocytosis, and the triggering of intracellular signaling pathways that modulate cell proliferation, survival, migration, invasion, cytokine production, and stimulation of angiogenesis [16–22]. Like testisin, PAR-2 expression is increased with ovarian cancer stage, with the highest PAR-2 expression occurring in stage IV tumors [17, 19, 23], where its expression correlates with decreased patient survival [17, 23]. Increased PAR-2 expression in ovarian tumors is associated with increased microvessel density and also increased tumor cell proliferation suggesting PAR-2 may function to enhance ovarian cancer angiogenesis [17], consistent with its role in other cancers [18, 24, 25].

The function of increased testisin in ovarian cancer metastasis is not known. Here we investigated the effect of increased testisin expression and activity in ovarian tumor cells using a preclinical xenograft model of late-stage ovarian tumor metastasis. Unexpectedly, we find that increased testisin activity has little effect on tumor cell proliferation, but suppresses intraperitoneal tumor dissemination and ascites accumulation resulting in reduced metastatic tumor burden relative to control cells. Testisin activity antagonized the synthesis and secretion of the proangiogenic factors angiopoietin (ANG)-2 and angiopoietin-like (ANGPTL)-4 and was associated with loss of cell surface PAR-2 and suppression of cytokine signaling. Together with the published literature, these results may suggest that successful metastasis requires the dampening of testisin expression at later stages of ovarian tumor metastasis, thereby promoting pro-angiogenic and pro-metastatic signaling. These data reveal a new complexity in the proteolytic mechanisms regulating epithelial ovarian tumor metastasis.

Materials and methods

Plasmids, antibodies, and other reagents

pDisplay-HA-testisin plasmids encoding both WT testisin and the S238A mutant were previously described [15]. pCDH-EF1-MCS-IRES-Puro was purchased from Systems Biosciences (Palo Alto, CA) and the pCMV-ΔR8.2 packaging plasmid and pCMV-VSVg envelope plasmid were purchased from Addgene (Cambridge, MA). Dr. Stuart Martin (University of Maryland School of Medicine) generously provided the pMSCV-Luciferase PGK-Hygro luciferase plasmid. Primary antibodies used were as follows: rabbit anti-human influenza hemagglutinin (HA) tag (Abcam, Cambridge, MA), mouse anti-PAR-2 (SAM11, EMD Millipore, Burlington, MA), rabbit anti-β-tubulin (Santa Cruz, Santa Cruz, CA), rabbit anti-phospho-ERK1/2, rabbit anti-total ERK1/2 (Cell Signaling Technologies, Danvers, MA), and rabbit anti-CD31 (Abcam). Mouse anti-testisin primary antibody D9.1 was isolated from PTA-6077 hybridoma cell line (Pro104.D9.1; ATCC, Manassas, VA). Secondary antibodies utilized were HRP-conjugated anti-mouse and anti-rabbit antibodies (Jackson ImmunoResearch Laboratories, West Grove, PA).

Cell culture

Human ovarian clear cell carcinoma ES-2 and the ovarian adenocarcinoma OVCAR3, CaOV3, and SKOV3 cell lines were purchased from American Type Culture Collection (ATCC, Manassas, VA). The human ovarian carcinoma cell line, NCI/ADR-Res, was purchased from the National Cancer Institute Division of Cancer Treatment and Diagnosis

(Bethesda, MD) and A2780 cells purchased from Sigma-Aldrich (St. Louis, MO). All cell lines were cultured and maintained at 37 °C in a 5% CO_2/95% air environment in Dulbecco's modified Eagle's medium (DMEM) or Roswell Park Institute Medium-1640 (RPMI-1640) (NCI/ADR-Res and A2780) supplemented with 10% heat-inactivated fetal bovine serum (FBS) and 100 units/mL penicillin, 100 μg/mL streptomycin, and 2 mM L-glutamine. Cell lines were mycoplasma negative by routine testing. Pharmacological inhibition of PAR-2 was performed by treating cells with 50 μM of the reversible PAR-2 antagonist GB83 (Axon Medchem, Reston, VA) or DMSO control for 24 h prior to analysis by quantitative real-time PCR (qPCR).

Development of an ovarian ES-2-luciferase reporter cell line

The ES-2 ovarian cancer cell line was labeled with luciferase for in vivo imaging. Conditioned media from Phoenix-AMPHO cells (ATCC) transfected with the retroviral expression plasmid pMSCV-Luciferase PGK-Hygro using Lipofectamine 2000 (ThermoFisher, Waltham, MA) were centrifuged and passed through a pre-wet 0.45-μm filter. ES-2 cells were transduced by application of cleared retroviral supernatants mixed with 6 μg/mL polybrene (AmericanBio, Natick, MA). A cell line stably expressing luciferase was selected by hygromycin and used for transfection experiments. Luciferase activity was assayed using 250 μg/mL D-luciferin (Perkin-Elmer, Waltham, MA) and the detection of luminescence with a Berthold Technologies Centro LB-960 plate reader and was normalized for cell number.

Expression of testisin in ES-2-Luc and OVCAR3 ovarian cancer cells

Lentiviral plasmids for expressing full-length testisin and the catalytically inactive testisin mutant S238A were generated by amplifying cDNA by PCR from expression plasmids containing an HA-tagged testisin (pDisplay.Testisin and pDisplay.TestisinSA) [15]. PCR products were purified and digested with restriction enzymes *Xba*I and *Nhe*I (New England Biolabs, Ipswich, MA). DNA was cloned into the *Xba*I–*Nhe*I sites of pCDH-EF1-MCS-IRES-Puro lentiviral expression vector and the plasmid transformed into DH5α competent cells (Life Technologies, Carlsbad, CA). Plasmid DNA was isolated from ampicillin-resistant colonies and confirmed by DNA sequencing (Biopolymer/Genomics Core Facility, University of Maryland School of Medicine). To produce lentiviral particles, HEK293T cells were transfected with a mixture of plasmids: pCMV-ΔR8.2 packaging plasmid, pCMV-VSVg envelope plasmid, and each generated pCDH-EF1-MCS-IRES-Puro vector or vector alone using Lipofectamine 2000. The lentiviral supernatants were collected 48 h after transfection, cleared by centrifugation at 2000*g* for 10 min and passed through a 0.45-μm filter. Lentiviral particles were mixed with 6 μg/mL polybrene and applied to ES-2-Luc cells. Pools of stably transduced cell lines expressing wild-type testisin (ES-2-Luc-TsWT), the catalytically inactive S238 mutant (ES-2-Luc-TsMut), and vector alone (ES-2-Luc-Ctl) were obtained by selection in puromycin. Several independent lines were generated and characterized to avoid any possibility of artifacts. Retention of luciferase in the stable ES-2-Luc cell lines was determined by analysis of luciferase mRNA by qPCR.

OVCAR3 cells were transiently transfected with 5 μg pDisplay-HA-WT Testisin (OVCAR3-TsWT), pDisplay-HA-Testisin S238A (OVCAR3-TsMut), or vector alone (OVCAR3-Ctl) using the NEON transfection system (ThermoFisher). Electroporation was performed following the manufacturer's instructions using the following conditions: 1050 V for 30 ms for two pulses. Electroporated cells were plated into antibiotic-free DMEM overnight, after which media was changed to complete DMEM.

xCELLigence cell proliferation assay

The xCELLigence RCTA system (ACEA Biosciences, San Diego, CA) was utilized to measure cell proliferation. ES-2-Luc cell lines were plated onto an E-plate and cell impedance, a measure of the number of cells and cell spreading, was measured every 30 min for up to 72 h per manufacturer instruction. Cell doubling time was calculated using RTCA 2.1.0 Software (ACEA Biosciences). Cells were maintained at 37 °C in a 5% CO_2/95% air environment throughout the experiment.

Murine xenograft model of ovarian cancer metastasis

Metastasis model ES-2-Luc-TsWT, ES-2-Luc-TsMut, and ES-2-Luc-Ctl cell lines (5×10^6 cells in 200 μL PBS) were injected into the peritoneal cavity of groups of female athymic nude mice (Nu/Nu) (seven mice/group; 6–8 weeks old) (Envigo, East Millstone, NJ). Tumor seeding was monitored at 4 days post injection by in vivo bioluminescent imaging in real time using the Xenogen IVIS-200. Mice showing equal average metastatic tumor burden (such that the mean photon intensity was similar) constituted each cohort of five mice and the groups were monitored for tumor progression thereafter. Body weight was recorded daily throughout the course of the experiments. Mice were monitored by body condition score (BCS) index and clinical evaluations, and euthanized if they showed either a > 10% increase in body weight compared to pre-injection body weight or if their activity level decreased due to accumulation of ascites and metastatic tumor burden. All procedures performed in studies involving animals were in accordance with the ethical standards of the University of

Maryland School of Medicine Institutional Animal Care and Use Committee (IACUC), the institution at which the studies were conducted.

Monitoring of metastatic tumor burden For in vivo bioluminescence imaging, 150 mg/kg D-luciferin was injected into the peritoneal cavity, and mice were returned to their cage to move freely for 3 min prior to imaging to ensure proper biodistribution of D-luciferin. Mice were anesthetized using isoflurane and anesthesia was maintained after placement in the Xenogen IVIS-200 chamber. Photon intensity was measured every 5 min, for up to 30 min, after luciferin injection. Peak total photon flux (photons/s) was determined and corrected for tissue depth by spectral imaging using Living Image 3.0 software (Xenogen, Alameda, CA). After the final day of imaging (day 12), mice were euthanized, and necropsies were performed. The peritoneal cavity of each mouse was opened by a small incision and ascites collected by pipet. The volume of ascites was measured using graduated vials. Ascites samples were briefly centrifuged to collect cells and ascites fluid. The cells were resuspended in ACK lysis buffer (Quality Biologicals, Gaithersburg, MD) to lyse the red blood cells and then snap-frozen for RNA analyses. The peritoneal cavity was then fully opened and peritoneal organs including the diaphragm and mesentery arteries were photographed using a Leica M80 stereo microscope and DMC4500 microscope camera. Organs collected from mice were fixed in 4% paraformaldehyde and processed for paraffin embedding for histological analysis. In some cases, tumor tissues were scraped from organs with forceps and snap-frozen for RNA and protein analyses.

Histopathological analyses

Tissues were fixed in 4% paraformaldehyde overnight and then stored in 70% ethanol. The specimens were then embedded in paraffin and 5-μm-thick sections were cut, deparaffinized, and stained with hematoxylin and eosin (H&E) using standard procedures, or subjected to immunohistochemical analysis. Briefly, formalin-fixed sections were deparaffinized in xylene, rehydrated in a graded series of ethanol, and washed in 1× Tris-buffered saline (TBS). Heat-induced antigen retrieval was performed on all sections using citrate buffer pH 6.0. After antigen retrieval, sections were washed twice in TBS, blocked for 1 h at room temperature with 10% goat serum + 1% BSA in TBS and incubated overnight at 4 °C with a primary antibody specific for CD31 (rabbit polyclonal, 1:50, Abcam) diluted in 1% BSA in TBS. Hydrogen peroxidase blocking with 0.3% H_2O_2 in TBS was performed after primary antibody incubation. Sections were washed twice and incubated with biotinylated secondary antibody for 1 h at room temperature. Detection of specific antigens was performed by development with Vectastain Elite ABC Kit (Vector Laboratories). Sections were incubated with diaminobenzidine (DAB) substrate-chromogen solution for 4.5 min. Slides were counterstained with hematoxylin prior to being dehydrated and mounted with PermaMount. Images of slides were obtained by the EVOS FL Auto Cell Imaging System (Life Technologies). All tissues were completed in a single run for consistency.

Quantitative real-time PCR

RNA was isolated from tumor cell lines or tumor tissues using the PureLink RNA mini kit (ThermoFisher) or the RNeasy mini kit (Qiagen, Germantown, MD) and cDNA generated by reverse transcription with the High Capacity Reverse Transcription kit (ThermoFisher). qPCR was performed utilizing TaqMan Master Mix and reactions analyzed using either the QuantStudio 3 (ThermoFisher) or 7900HT PCR system (Applied Biosystems, Foster City, CA). TaqMan primers against testisin (Hs00199035_m1), luciferase (Mr03987587_mr), ANGPTL4 (Hs01101127_m1), ANG2 (Hs01048042_m1), ANG1 (Hs00375823_m1), PECAM1 (Hs01065279_m1), VEGFA (Hs00900055_ml), PDGFB (Hs00966522), TIE2 (Hs00945150), PAR-2 (Hs00608346_m1), IL-8 (Hs00174103_m1), and GAPDH (4325792) were purchased from ThermoFisher. For ANGPTL2, qPCR was performed with SYBR Green reagents on the QuantStudio 3 using the primers: forward 5′-GCCA CCAAGTGTCAGCCTCA-3′ and reverse 5′-TGGA CAGTACCAAACATCCAACATC-3′. The Human Angiogenesis TaqMan array (ThermoFisher), containing 92 genes associated with vascular function, was probed by qPCR using RNA isolated from ES-2-Luc-TsWT and ES-2-Luc-Ctl cell lines. mRNA expression was normalized to GAPDH. The TissueScan Ovarian Cancer cDNA Array II (II (HORT502; Origene) containing 48 samples covering four disease stages of varying histopathologies, and normal tissues were screened for testisin and PAR-2 mRNA gene expression using TaqMan Master Mix and the primers listed above.

Immunoblot analysis

Cell lines and tumor tissues were lysed in cell lysis buffer (0.5% Triton X-100, 0.5% NP40, 60 mM HEPES (pH 7.3), 150 mM NaCl, Complete Mini Protease Inhibitor Cocktail & PhosSTOP Phosphatase Inhibitor Cocktail (Roche, Indianapolis, IN)). Protein concentrations were determined by Bradford assay utilizing Protein Assay Dye (Bio-Rad, Hercules, CA) and samples containing equal protein were prepared with 1X LDS sample buffer containing 7% β-mercaptoethanol and heated at either 95 °C for 3 min or for PAR-2, 70 °C for 10 min. Samples were separated by SDS-polyacrylamide gel electrophoresis on either a 4–12% or 12% Bis Tris NuPage Gel (ThermoFisher). Samples were

transferred by immunoblot to 0.45 μm PVDF membrane (EMD Millipore) and blocked in either 5% milk or bovine serum albumin (*w*/*v*). Membranes were probed with primary antibodies overnight at 4 °C and then HRP-conjugated secondary antibodies for 1 h at room temperature. HRP activity was detected by SuperSignal West Pico PLUS Chemiluminescent Substrate (ThermoFisher).

ELISA

Cells were seeded overnight, media replaced, and conditioned media collected after 24 or 48 h. The conditioned media and ascites fluids from mice were centrifuged to remove any remaining cells or debris and analyzed using the human ANG2 Quantikine ELISA kit (R&D Systems, Minneapolis, MN) or human ANGPTL4 ELISA kit (ThermoFisher) according to manufacturers' instructions. Signals were measured by absorbance at 450 nm using a FlexStation 3 Multi-Mode Microplate Reader (Molecular Devices, San Jose, CA) and the concentration of samples interpolated from included standards.

Fluorogenic peptide cleavage assay

Ovarian tumor cell lines grown overnight in 96-well, black-walled, clear-bottom plates were incubated with 100 μM BOC-QAR-AMC peptide (R&D Systems) in the presence or absence of 100 μM AEBSF (Sigma-Aldrich, St. Louis, MO) in Opti-MEM media. Proteolytic cleavage of the peptide and release of the AMC group was assayed by the change in fluorescence measured over time up to 24 h after the addition of the peptide using the FlexStation 3 (excitation: 380 nm; emission: 460 nm). Wells containing BOC-QAR-AMC alone or BOC-QAR-AMC and AEBSF alone were included as controls and subtracted from results as background.

siRNA knockdown studies

For testisin siRNA knockdown, cells were transfected with 20 nM of the Stealth RNAi targeted against testisin (siTS94 (HSS116894) and the Silencer Select siRNA (siTs67 (s223167; ThermoFisher) or 20 nM of a nonspecific control (Stealth RNAi targeted against luciferase (12935146; ThermoFisher)) for up to 120 h. Knockdown of testisin in the cells was confirmed by qPCR. For silencing of PAR-2, originally three Stealth siRNAs (s223507, s4295, and s4296; ThermoFisher) targeted against PAR-2 were tested for their abilities to specifically knockdown PAR-2 expression. A siRNA pool of the two nonredundant-specific siRNAs (s223507 and s4296) and a nonredundant third independent Silencer Select siRNA siPAR-2 #26 (s4926, ThermoFisher) were used for siRNA knockdown studies. Cells were treated with either the PAR-2 siRNAs (50 nM each) or the nonspecific control (100 nM) for 96 h. Effective knockdown of PAR-2 in each of the cell lines was confirmed at the level of protein by Western blot and RNA by qPCR. All transfections were carried out with DharmaFECT 1 transfection reagent (Dharmacon, Lafayette, CO).

Flow cytometry

Cells were washed in PBS and then lifted from plates by treatment with Versene (ThermoFisher). For the detection of total PAR-2, cells were fixed in 4% paraformaldehyde for 10 min at room temperature and permeabilized using 0.5% Triton X-100. For the detection of cell surface PAR-2, cells were maintained in ice-cold FACS buffer (PBS pH 7.4, 0.5% FBS, and 0.025% sodium azide). Cells were then washed twice in ice-cold FACS buffer and incubated with an anti-PAR-2 antibody (SAM11) (EMD Millipore) on ice for 30 min. Cells were again washed in FACS buffer and incubated with AlexaFluor 488 secondary antibody (Invitrogen) for 15 min on ice. Following secondary antibody incubation, cells were stained with propidium iodide (PI) (Roche) and PI-positive cells were excluded by negative gating. Single cells were identified by light scatter profile and analyzed for PAR-2 expression. Flow cytometry data were acquired using a LSR Fortessa (BD Biosciences) and analyzed with FlowJo software (FlowJo, LLC).

Statistical analysis

Data are presented as means with standard error (SEM). Comparison of experimental groups was performed by either one-sample *t* test, Student's two-tailed *t* test, or one-way repeated measure analysis of variance (ANOVA) followed by Tukey's multiple comparison test. Data was analyzed utilizing GraphPad software (GraphPad Prism 5.01), and p values < 0.05 were considered statistically significant.

Results

Association of testisin with ovarian cancer

Gene expression profiling of testisin in human ovarian cancer patient tissues showed that testisin is frequently increased in cancer tissues at all stages of ovarian cancer progression, relative to the undetectable levels in normal ovarian samples (Fig. 1a), which is consistent with studies by others [7, 14]. To generate a suitable cell model to investigate testisin's function in ovarian cancer, we surveyed a series of ovarian cancer cell lines for testisin expression by qPCR and immunoblotting (Fig. 1b). We found that the epithelial ovarian cancer cell lines, CaOV3, and NCI/ADR-Res expressed the highest levels of testisin, whereas the human clear cell ovarian carcinoma ES-2, human ovarian adenocarcinoma cell lines OVCAR3

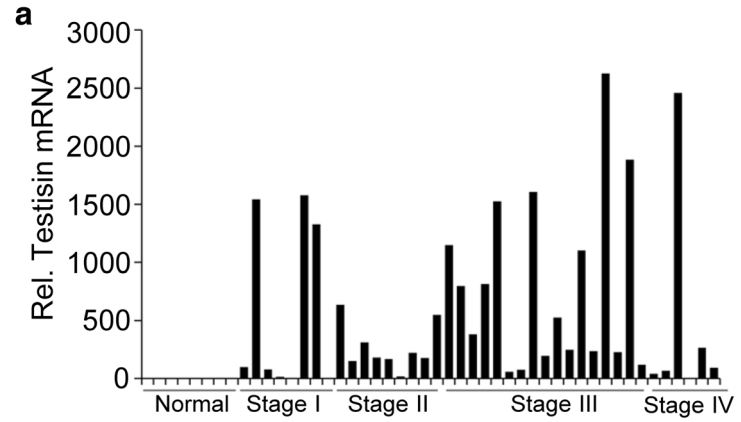
a
Rel. Testisin mRNA
3000
2500
2000
1500
1000
500
0
Normal
Stage I
Stage II
Stage III
Stage IV

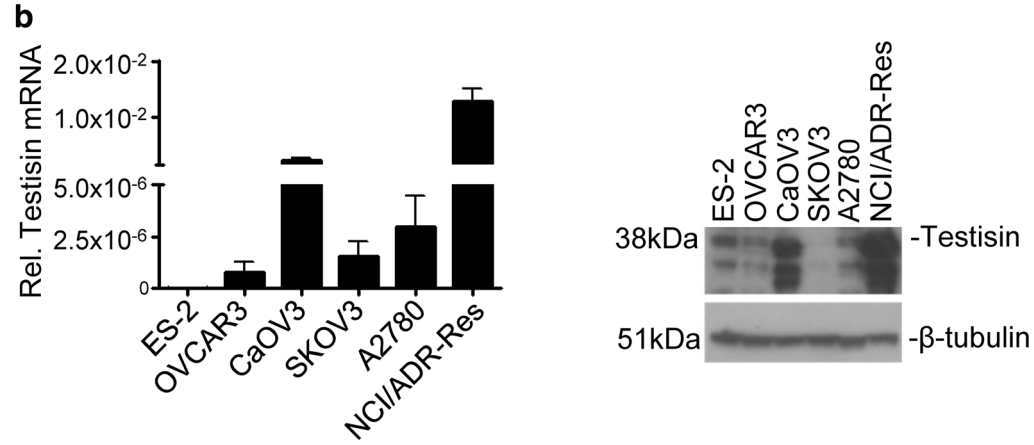
b
Rel. Testisin mRNA
2.0x10-2
1.0x10-2
5.0x10-6
2.5x10-6
0
ES-2
OVCAR3
CaOV3
SKOV3
A2780
NCI/ADR-Res
38kDa
-Testisin
51kDa
-β-tubulin

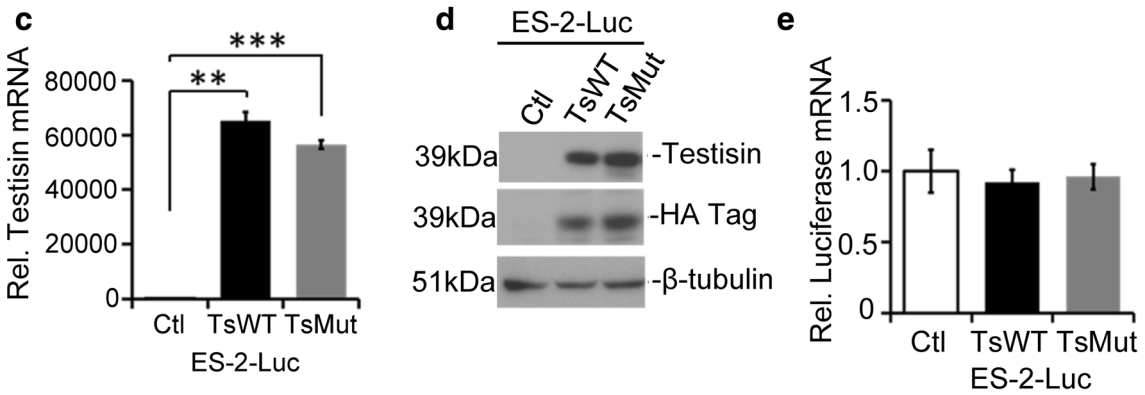
c
Rel. Testisin mRNA
80000
60000
40000
20000
0
***
**
Ctl
TsWT
TsMut
ES-2-Luc
d
ES-2-Luc
Ctl
TsWT
TsMut
39kDa
-Testisin
39kDa
-HA Tag
51kDa
-β-tubulin
e
Rel. Luciferase mRNA
1.5
1.0
0.5
0
Ctl
TsWT
TsMut
ES-2-Luc

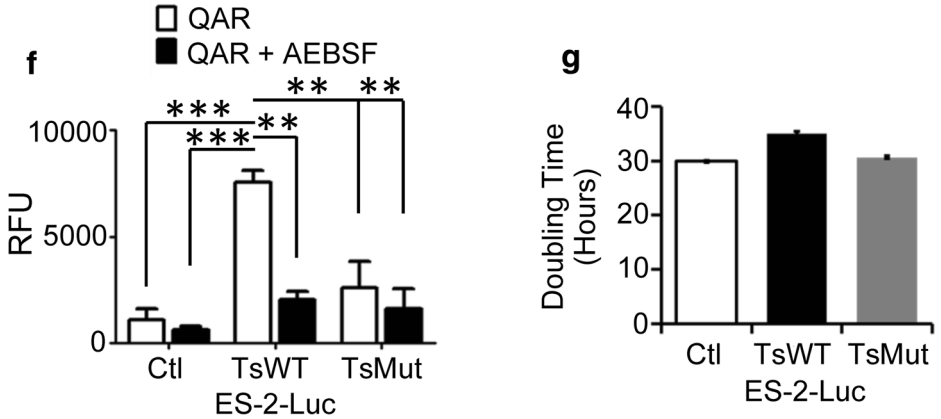
f
QAR
QAR + AEBSF
RFU
10000
5000
0
***
***
**
**
**
Ctl
TsWT
TsMut
ES-2-Luc
g
Doubling Time (Hours)
40
30
20
10
0
Ctl
TsWT
TsMut
ES-2-Luc

◀ **Fig. 1** Testisin expression in human ovarian cancers. **a** Testisin mRNA expression in 40 human ovarian cancer patient tissues compared with 8 normal human ovarian tissues across all stages of the disease using the TissueScan RealTime Ovarian Cancer Panel II. Tissue samples are normalized to one another using the house-keeping gene, β-actin. **b** Total RNA from six ovarian cancer cell lines (ES-2, OVCAR3, SKOV3, NCI/ADR-Res, A2780, and CaOV3) was isolated and analyzed by qPCR for testisin expression (*left panel*). mRNA expression levels are relative to GAPDH expression. Results are from technical replicates performed in triplicate. Immunoblot analysis of cell lysates prepared from the ovarian cancer cell lines (*right panel*). Blots were probed with antibodies against testisin and β-tubulin. **c** qPCR analysis of mRNA isolated from ES-2-Luc-TsWT, ES-2-Luc-TsMut, or ES-2-Luc-Ctl. The graph represents the mean ± SEM from two independent experiments. $^{**}p < 0.01$; $^{***}p < 0.001$, unpaired *t* test. **d** Immunoblot analysis of cell lysates prepared from ES-2-Luc-TsWT, ES-2-Luc-TsMut, or ES-2-Luc-Ctl cell lines probed with antibodies against testisin, HA, and β-tubulin. The HA tag increases the molecular weight of testisin to ~39kDa. The data is representative of two independent experiments. **e** qPCR analysis of luciferase mRNA expression in ES-2-Luc-TsWT, ES-2-Luc-TsMut, and ES-2-Luc-Ctl cells showing that luciferase expression is equally retained across all of the transduced cell lines. Signals are normalized to GAPDH and expressed relative to ES-2-Luc-Ctl cells. The data is representative of two independent experiments. $^{*}p < 0.05$; $^{**}p < 0.01$; $^{***}p < 0.001$, unpaired *t* test. **f** ES-2-Luc-TsWT cells show significantly increased cell surface proteolytic activity as measured using the fluorogenic peptide BOC-QAR-AMC in the presence or absence of the serine protease inhibitor AEBSF. Graph shows mean ± SEM and is representative of three independent experiments. $^{*}p < 0.05$; $^{**}p < 0.01$; $^{***}p < 0.001$, one-way ANOVA with post hoc Tukey's test. **g** The rate of ES-2-Luc cell proliferation was determined by measuring cell doubling time utilizing the xCELLigence RTCA system. Results are from technical replicates performed in triplicate

and SKOV3, and the human ovarian carcinoma A2780 cell lines expressed low to negligible levels (Fig 1b).

To evaluate the effect of increased testisin expression in ovarian tumors, an orthotopic murine intraperitoneal xenograft model was developed using luciferase-labeled ES-2 cells (ES-2-Luc) to facilitate imaging of tumor metastasis in vivo. We generated a panel of ES-2-Luc cell lines expressing (1) HA-tagged wild-type testisin (ES-2-Luc-TsWT), (2) a catalytically inactive mutant form of testisin (ES-2-Luc-TsMut), or (3) vector alone (ES-2-Luc-Ctl). The S238A mutation in ES-2-Luc-TsMut replaces the nucleophile Ser^{238} of the testisin catalytic triad with Ala^{238}, abrogating the ability of the protease to cleave a peptide substrate [15]. The HA-tag is positioned at the N-terminus of testisin for ease of detection and has been shown not to affect testisin activity or cell surface expression [15]. The expression of testisin in these cell lines was confirmed by qPCR (Fig. 1c) and immunoblot (Fig. 1d) analyses. Both ES-2-Luc-TsWT and ES-2-Luc-TsMut lines overexpress similar levels of testisin and mutant testisin, respectively, compared with ES-2-Luc-Ctl, which has comparably very little endogenous testisin protein expression. The baseline luciferase expression levels were maintained in each of the three cell lines (Fig. 1e).

To confirm that the expressed wild-type testisin was active, cell surface proteolytic activity of each of the cell lines was measured by fluorogenic peptide assay (Fig. 1f), and this activity compared in the absence and presence of the serine protease inhibitor AEBSF, to specifically measure serine protease activity. The results show that testisins expressing ES-2-Luc-TsWT display ~ 7-fold increased proteolytic activity over cells expressing the controls, mutant testisin (ES-2-Luc-TsMut), and vector alone (ES-2-Luc-Ctl) (Fig. 1f).

Testisin proteolytic activity does not affect ES-2-Luc tumor growth, adhesion, or migration

The effect of testisin proteolytic activity on tumor cell growth was assayed using the xCELLIGENCE system. No effects of testisin expression on cell growth were observed, as measured by cell doubling time (Fig. 1g). To further evaluate the effect of testisin on tumor cell growth, ES-2-Luc-TsWT and ES-2-Luc-Ctl cells were implanted s.c into nude mice and in vivo tumor growth was monitored. No significant difference in tumor volumes or rates of xenograft tumor growth were observed between mice carrying ES-2-Luc-Ctl and ES-2-Luc-TsWT tumors (Supplementary Fig. 1). At the conclusion of the experiment, tumors were harvested and comparison of average tumor weights confirmed that the excised ES-2-Luc-Ctl and ES-2-Luc-TsWT tumors were not significantly different (Supplementary Fig. 1). In vitro experiments evaluating the effect of testisin activity on cell migration and rates of cell attachment also showed no significant differences in testisin expressing and control cell lines (Supplementary Fig. 2a&b).

Testisin proteolytic activity reduces metastatic tumor burden and development of ascites in a xenograft model of ovarian tumor metastasis

The intra-peritoneal (i.p.) ES-2-Luc xenograft model reproduces key events of late-stage ovarian cancer metastasis specifically requiring tumor cells to undergo peritoneal adhesion, sub-mesothelial anchoring, and invasion in order to establish a metastatic tumor foci [26]. To evaluate the effect of testisin activity on metastatic tumor processes, the ES-2-Luc-TsWT, ES-2-Luc-TsMut, and ES-2-Luc-Ctl cell lines were injected i.p. into nude mice and tumor seeding and progression were monitored by luminescence using the Xenogen in vivo imaging system (IVIS) for up to 12 days (Fig. 2a). Somewhat surprisingly, two independent experiments showed that mice carrying ES-2-Luc-TsWT tumors displayed *decreased* metastatic tumor burden by IVIS imaging compared with mice carrying either ES-2-Luc-TsMut or ES-2-Luc-Ctl tumors (Fig. 2a). Quantification of IVIS imaging shows that compared to mice carrying ES-2-Luc-Ctl tumors, mice carrying ES-2-Luc-TsWT tumors showed a 47% reduction in metastatic tumor burden at day 7 and a 67% reduction at day 12 (Fig. 2b), whereas mice carrying ES-2-Luc-TsMut tumors had a similar metastatic tumor burden as ES-2-Luc-Ctl mice,

Table 1 Angiogenic genes altered by constitutive testisin expression in ES-2-Luc-TsWT cells compared to ES-2-Luc-Ctl cells

Gene symbol	Assay ID	ΔC_T ES-Luc-Ctl	ΔC_T ES-Luc-TsWT	Fold change
Genes upregulated ≥ 2-fold				
PECAM1	Hs00169777_m1	15.98	13.96	4.05
CDH5	Hs00174344_m1	8.03	6.98	2.07
FST	Hs00246256_m1	7.05	6.00	2.07
EDIL3	Hs00174781_m1	14.01	12.98	2.04
IL12A	Hs00168405_m1	10.01	8.98	2.04
TNF	Hs00174128_m1	18.05	17.03	2.03
CXCL2	Hs00601975_m1	7.99	6.97	2.03
THBS1	Hs00962914_m1	8.00	6.98	2.03
Genes downregulated ≥ 2-fold				
ANGPTL4	Hs01101127_m1	13.07	16.02	7.76
PDGFB	Hs00234042_m1	12.01	14.03	4.05
ANGPTL2	Hs00765775_m1	14.02	16.02	4.01
KIT	Hs00174029_m1	13.00	15.00	4.01
PDGFRB	Hs00387364_m1	13.05	15.05	4.01
COL18A1	Hs00181017_m1	9.03	11.03	3.99
THBS2	Hs01568063_m1	16.05	18.01	3.90
TNNI1	Hs00913333_m1	17.03	18.28	2.38
COL4A3	Hs01022527_m1	14.89	16.13	2.36
EPHB2	Hs00362096_m1	6.96	8.01	2.06
FGF4	Hs00173564_m1	18.99	20.03	2.06
ITGA4	Hs00168433_m1	9.00	10.03	2.04
TYMP	Hs00157317_m1	15.00	16.02	2.03
HSPG2	Hs00194179_m1	9.01	10.02	2.02
PTN	Hs00383235_m1	12.03	13.04	2.02
TIE1	Hs00178500_m1	5.02	6.03	2.02
HEY1	Hs00232618_m1	12.02	13.02	2.00
ITGB3	Hs01001469_m1	7.01	8.01	2.00
FBLN5	Hs00197064_m1	19.00	20.00	2.00
ANGPT2	Hs00169867_m1	11.98	12.98	2.00

*Total RNA was isolated from ES-2-Luc-TsWT and ES-2-Luc-Ctl and analyzed by TaqMan Angiogenesis Signature Array (ThermoFisher) according to the manufacturers' instructions

demonstrating that testisin proteolytic activity is responsible for the reduction in metastatic tumor burden. Correlating with reduced metastatic tumor burden, the volume of accumulated ascites fluid collected from mice carrying ES-2-Luc-TsWT tumors was reduced by 86% compared to mice carrying ES-2-Luc-Ctl tumors (Fig. 2c). Mice carrying ES-2-Luc-TsMut tumors showed similar ascites production as mice carrying ES-2-Luc-Ctl tumors, indicating that expressed testisin proteolytic activity was required to diminish the development of ascites in this model.

Molecular analyses of testisin and luciferase mRNA expression in tumor tissues recovered from mouse diaphragms confirmed that ES-2-Luc-TsWT and ES-2-Luc-TsMut had retained similar levels of transgene expression (Fig. 2d), showing that the observed decrease in metastatic tumor burden was due to testisin activity and not a loss of testisin in the tumor xenografts. These results suggest a suppressor role for testisin activity in late stages of ovarian tumor metastasis.

Histological analysis of metastatic tumors in the ES-2-Luc intraperitoneal xenograft model

Metastatic tumor burden assessed at necropsy was widespread in mice carrying ES-2-Luc-Ctl tumors. Tumor cells covered the diaphragm, and the mesenteric arteries and multiple tumor nodules were dispersed throughout the abdominal cavity with additional metastatic foci observed attached to organs and the walls of the peritoneal cavity (Fig. 3a, b, ES-2-Luc-Ctl). These sites of metastasis frequently occur in relapsed and advanced

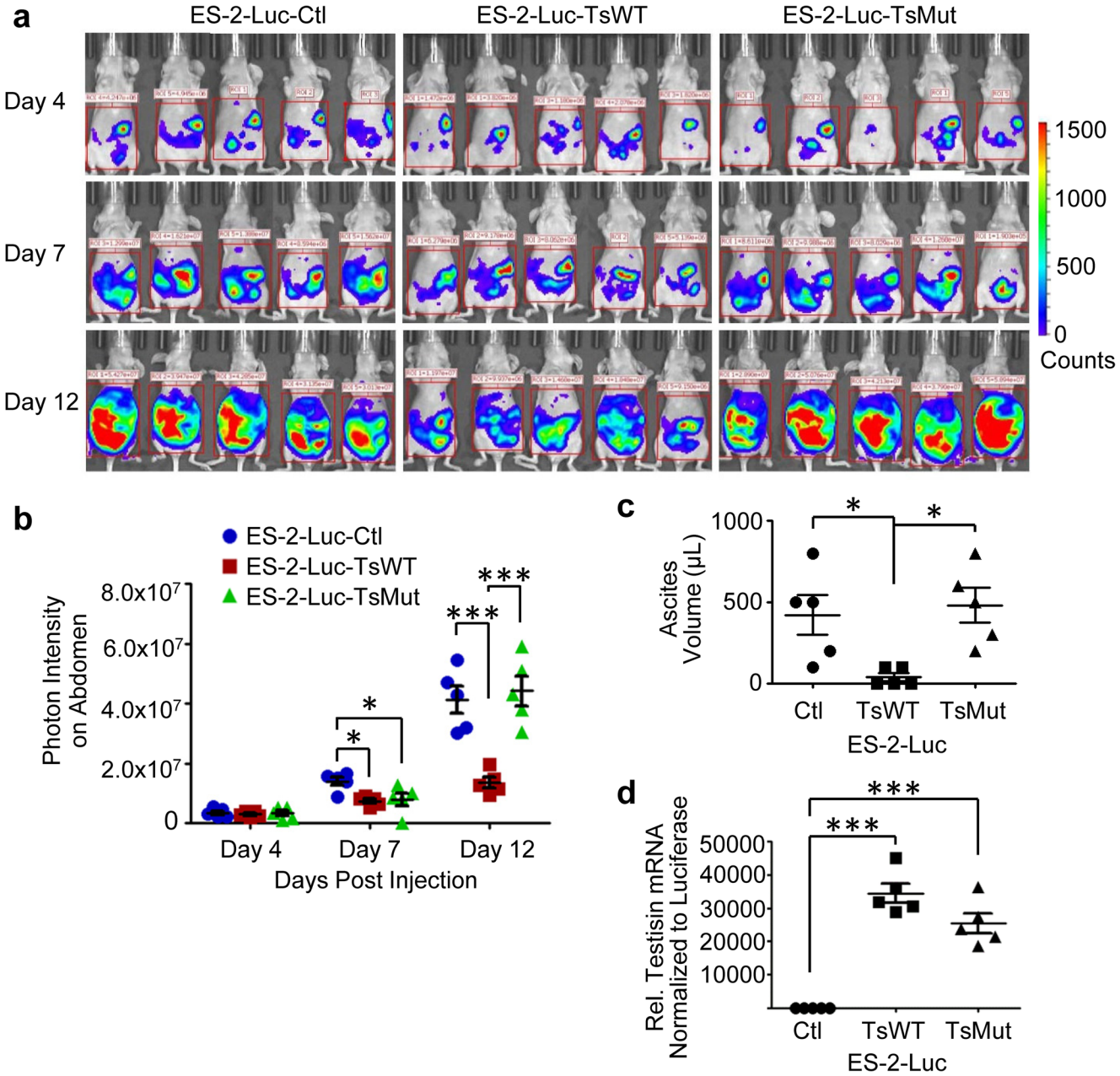

Fig. 2 Testisin expression reduces ovarian metastatic tumor burden in a manner dependent on proteolytic activity. **a** Cohorts of mice ($n = 5$) bearing ES-2-Luc-TsWT, ES-2-Luc-TsMut, or ES-2-Luc-Ctl i.p. xenograft tumors were monitored at days 4, 7, and 12 by in vivo bioluminescence imaging. Images represent the peak luciferase activity levels in the individual mice. **b** Quantification of bioluminescence in mice carrying ES-2-Luc-TsWT tumors compared to mice carrying ES-2-Luc-TsMut or ES-2-Luc-Ctl tumors. Results are representative of two independent experiments $n = 5$ mice per group; $^{*}p < 0.05$; $^{**}p < 0.01$; $^{***}p < 0.001$, one-way ANOVA with post hoc Tukey's test. **c** Volume of ascites recovered from the intraperitoneal cavities of mice carrying ES-2-Luc-TsWT, ES-2-Luc-TsMut, and ES-2-Luc-Ctl tumors. **d** Testisin expression is retained in in vivo ES-2-Luc-TsWT and ES-2-Luc-TsMut tumors. Tumor tissue samples collected from mouse diaphragms at necropsy were analyzed by qPCR for testisin mRNA relative to GAPDH. Signals were also normalized to luciferase mRNA expression in the tissue samples to normalize for tumor only, separate from non-tumor cells present in the xenograft tissues. Mice: $n = 5$ per group. $^{*}p < 0.05$; $^{**}p < 0.01$; $^{***}p < 0.001$, one-way ANOVA with post hoc Tukey's test

human ovarian cancers, indicating that this ES-2-Luc model, at least in part, reflects the biological behavior of a late-stage ovarian cancer [2].

Visual inspection of mice carrying ES-2-Luc-TsWT tumors at necropsy showed substantially reduced numbers and size of dispersed tumor nodules compared to mice carrying ES-2-Luc-Ctl tumors (Fig. 3a, b), consistent with the decreased signals detected by IVIS imaging. There was substantially less metastatic tumor burden around the mesenteric arteries, seen as an opalescent plaque covering the arteries (Fig. 3a) and reduced opalescent tumor foci and plaques on the diaphragm (Fig. 3b) compared to ES-2-

Luc-Ctl tumors. There were also fewer visible metastatic foci present on the liver surrounding the gall bladders, which were enlarged in mice carrying ES-2-Luc-Ctl and ES-2-Luc-TsMut (Fig. 3b, arrows), and on the peritoneal cavity wall (data not shown). This reduction in metastatic tumor burden was dependent on testisin activity, since mice carrying ES-2-Luc-TsMut tumors showed substantial metastatic foci indistinguishable from mice carrying ES-2-Luc-Ctl tumors (Fig. 3a, b). While mice carrying ES-2-Luc-TsWT tumors had significantly reduced metastatic tumor burden, histologic analysis of the few tumor foci identified on the diaphragm showed that tumor morphology and invasion to the diaphragm muscle was similar between all three tumor groups (Fig. 3c). Immunohistochemical staining of tumor tissues for the endothelial cell marker CD31 also indicates that tumors from all three groups are vascularized with vessels penetrating the tumor tissues and surrounding tumor cell clusters (Supplementary Fig. 3). The lack of obvious morphological differences between the three ES-2-Luc tumors may suggest that the few colonized ES-2-Luc-TsWT tumors were able to overcome the effect of testisin expression to metastasize to peritoneal organs. Together, the data suggest that testisin activity delays the propensity of ES-2-Luc cells to metastasize, an early event that may not be captured in the collected tumor samples.

Testisin targets PAR-2 on ES-2-Luc cells

Since PAR-2 is a target of testisin proteolytic activity, we sought to determine whether increased testisin may induce PAR-2 activation in the ES-2-Luc ovarian cancer cells. Cleavage of the PAR-2 activation site by testisin has been shown previously to induce PAR-2 internalization and prolonged loss of PAR-2 from the cell surface of HeLa cells [15]. To determine if testisin expressed in ES-2-Luc cells has a similar effect, cell surface and total expression of PAR-2 on ES-2-Luc-TsWT, ES-2-Luc-Ctl, and ES-2-Luc-TsMut cell lines were determined by flow cytometry (Fig. 4a). Surface PAR-2 expression was reduced by 85% in testisin expressing ES-2-Luc-TsWT cells, compared to ES-2-Luc-Ctl and ES-2-Luc-TsMut cells, indicating that testisin expression and activity facilitates PAR-2 internalization in ES-2-Luc cells (Fig. 4b). Total PAR-2 levels were unaffected by testisin expression or activity (Fig. 4b). A similar loss of PAR-2 with increased testisin expression was also reproduced using the OVCAR3 ovarian cancer cell line (Supplementary Fig. 4). These data show that increased testisin expression cleaves PAR-2, inducing increased turnover of PAR-2 from the cell surface, and provide support for the involvement of PAR-2 in the testisin-mediated functional effects on ES-2-Luc cells.

Testisin activity on ES-2-Luc cells suppresses PAR-2 downstream signaling

PAR-2 activation regulates an array of pro-inflammatory cytokines and chemokines such as IL-8 (*CXCL8*) [27]. IL-8 is consistently upregulated in ovarian cancers and is associated with angiogenesis, invasion, metastasis, and poor survival in ovarian and other cancers [28–30]. To determine the effect of testisin proteolytic activity on IL-8 expression in ES-2-Luc cells, IL-8 mRNA levels were measured by qPCR. ES-2-Luc-TsWT cells showed a significant two-fold decrease in IL-8 expression compared to the ES-2-Luc-Ctl cells (Fig. 4c) indicating that testisin activity suppressed IL-8 expression. Since previous studies have shown that PAR-2 activation stimulates IL-8 synthesis and release via activation of ERK1/2 signaling [31], the effect of testisin proteolytic activity on ERK1/2 activation in the ES-2-Luc cells was also examined (Fig. 4d). ERK1/2 phosphorylation was significantly reduced in testisin-expressing ES-2-Luc-TsWT by 42%, compared to ES-2-Luc-Ctl and ES-2-Luc-TsMut cells, while total ERK levels were unaffected (Fig. 4d). These data implicate increased testisin proteolytic activity in suppressing ERK1/2 activation and IL-8 production downstream of PAR-2.

Testisin activity reduces ANG2 and ANGPTL4 production in ES-2-Luc cells

As testisin proteolytic activity in the ES-2-Luc xenograft model resulted in reduced accumulation of ascites and also reduced expression of IL-8, which has been shown to promote angiogenesis in ovarian and other cancers [29, 32, 33], we investigated the possibility that testisin may modulate additional genes involved in the regulation of vascular permeability and/or angiogenesis. A global screen of angiogenesis genes was performed using the TaqMan human angiogenesis array. Genes whose expression changed by at least two-fold in the ES-2-Luc-TsWT line compared to ES-2-Luc-Ctl are listed in Table 1. PECAM1 (CD31) was upregulated in ES-2-Luc-TsWT cells, while several members of the angiopoietin and angiopoietin-like family were differentially downregulated in ES-2-Luc-TsWT cells including those encoding the pro-angiogenic proteins ANG2 and ANGPTL4. Validation of the array results by qPCR confirmed the significant decrease in expression of both ANG2 and ANGPTL4 mRNAs, by five-fold and three-fold, respectively, in testisin expressing ES-2-Luc-TsWT cells compared with ES-2-Luc-Ctl or ES-2-Luc-TsMut cells (Fig. 5a). PECAM1 mRNA was differentially upregulated by ~2-fold in ES-2-Luc-TsWT cells compared with both ES-2-Luc-Ctl and ES-2-Luc-TsMut cells. No

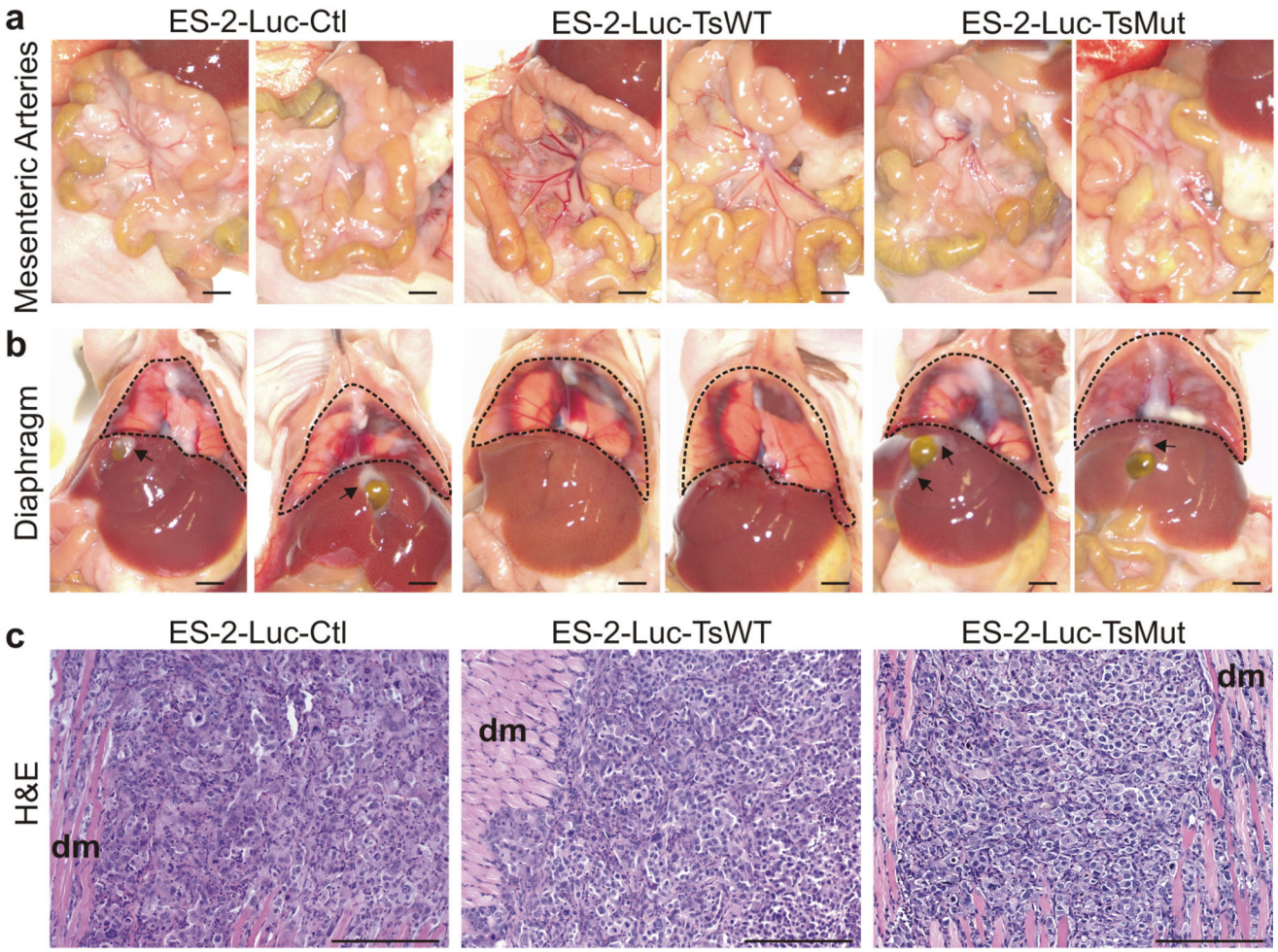

Fig. 3 Metastatic tumor burden is decreased in mice carrying tumors expressing testisin activity. Representative photographs of peritoneal organs taken at necropsy showing widespread, multiple tumor nodules attached to major sites of ES-2-Luc metastasis, the **a** mesenteric arteries and **b** diaphragm (outlined by dotted line). Substantially, fewer tumor cells and tumor nodules were observed in mice carrying ES-2-Luc-TsWT compared to the ES-2-Luc-TsMut and ES-2-Luc-Ctl tumors, consistent with IVIS imaging. Tumors appear as opalescent white plaques covering the lining of the organs and obscuring the mesenteric arteries. Arrows indicate tumor foci on the liver surrounding the gall bladder. Gall bladders were also substantially enlarged in mice carrying ES-2-Luc-Ctl tumors compared to mice carrying ES-2-Luc-TsWT tumors. Necropsy images are representative of the metastatic tumor burden in each of the respective cohorts of mice. Scale bar equals 2 mm. **c** Histologic analyses. Representative H&E staining of diaphragm tissues show tumor foci that have invaded into the diaphragmatic muscle (indicated by **dm**), with no obvious difference in the microscopic appearance between the three tumor lines. Scale bar equals 200 μm

significant changes in ANG1 and ANGPTL2 mRNA resulting from increased testisin expression were detected. Several other angiogenesis-related genes that were identified as differentially expressed in the array were not validated by qPCR (Fig. 5a). Consistent with the downregulation of ANG2 and ANGPTL4 at the mRNA level, we found that secreted ANG2 protein in culture media assayed by ELISA was significantly decreased by ~3-fold in ES-2-Luc-TsWT cells (Fig. 5b), and ANGPTL4 protein levels were also significantly decreased although to a lesser extent (Fig. 5b). These results demonstrate a novel activity for testisin in suppressing the synthesis and secretion of both ANG2 and ANGPTL4.

Testisin activity antagonizes ANG2 and ANGPTL4 expression in other ovarian tumor lines

To determine if the regulation of PECAM1, ANG2, and ANGPTL4 by testisin occurs more generally in other ovarian cancer cells, besides ES-2-Luc cells, we expressed WT testisin, catalytically inactive testisin or vector alone, in OVCAR3 cells. Testisin expression was confirmed by immunoblot (Fig. 6a). Increased testisin expression in OVCAR3 cells did not replicate increased PECAM1 expression observed in ES-2-Luc cells, and therefore, PECAM1 was not studied further (Fig. 6b). Notably, testisin expressing OVCAR3-TsWT cells showed significantly reduced mRNA levels of both ANGPTL4 (Fig. 6c) and ANG2 (Fig. 6d)

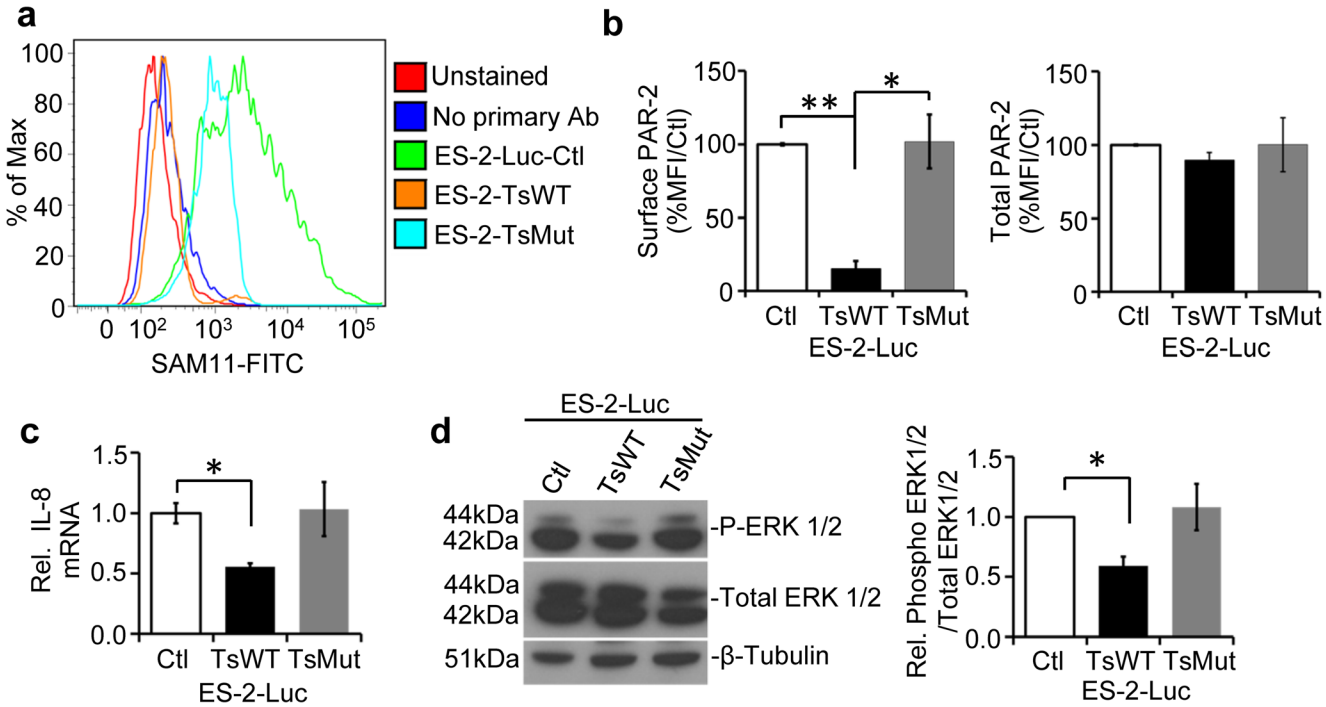

Fig. 4 Testisin targets PAR-2 on the surface of ES-2-Luc ovarian cancer cells. **a** Representative flow cytometry of non-permeabilized ES-2-Luc-TsWT, ES-2-TsMut, and ES-2-Luc-Ctl cells stained for surface PAR-2 expression using the SAM11 antibody. Unstained cells or those stained without primary antibody served as negative controls. The surface PAR-2 expression in the presence of testisin was similar to the negative control cells, indicating a significant loss of PAR-2 cell surface expression accompanies increased testisin expression in the ES-2-Luc cells. **b** Quantification of fluorescent signals show the significant loss of PAR-2 from the surface of ES-2-Luc-TsWT cells compared to ES-2-Luc-Ctl or ES-2-Luc-TsMut. Total PAR-2 expression, measured in permeabilized cells by flow cytometry, was similar for ES-2-Luc-TsWT cells, ES-2-Luc-Ctl, and ES-2-Luc-TsMut cells. Graphs are mean ± std. error from two independent experiments, $*p < 0.05$; $**p < 0.01$, unpaired *t* test. **c** qPCR analysis of mRNA isolated from ES-2-Luc-TsWT, ES-2-Luc-TsMut, or ES-2-Luc-Ctl demonstrates testisin proteolytic activity significantly reduces expression of IL-8 compared to ES-2-Luc-Ctl cells. The graph represents the mean ± SEM from three independent experiments. $*p < 0.05$, unpaired *t* test. **d** Western blot analysis of ERK1/2 activation in ES-2-Luc-TsWT, ES-2-Luc-TsMut, and ES-2-Luc-Ctl cell lines. Blots were probed with antibodies against phosphorylated-ERK1/2 and total ERK1/2. Graph shows densitometric analysis of phosphorylated ERK1/2 protein relative to total ERK1/2 after normalizing to β-tubulin. Graphs show mean ± SEM and are the average of at least two independent experiments. $* p < 0.05$, unpaired *t* test

compared to control OVCAR3-Ctl cells, a finding similar to that observed in the corresponding ES-2-Luc cells.

To further investigate the regulation of ANG2 and ANGPTL4 by testisin, testisin siRNA knockdown was performed in NCI/ADR-Res ovarian cancer cells, which express endogenous testisin (Fig. 1b). Knockdown of testisin in the NCI/ADR-Res cell line using two nonredundant siRNAs significantly increased the expression of ANG2 and ANGPTL4 (Fig. 6f, g). Together, these data provide strong support for modulation of the expression of ANG2 and ANGPTL4 by testisin activity.

PAR-2 is involved in testisin-induced downregulation of ANG2 and ANGPTL4

Since we had previously found that testisin activity enhanced the PAR-2 internalization and loss from the cell surface, and also suppressed PAR-2 downstream signaling (Fig. 4), we used siRNA silencing of PAR-2 to investigate whether PAR-2 may play a role in testisin-induced downregulation of ANG2 and ANGPTL4 (Fig. 7a). Loss of PAR-2 by siRNA knockdown significantly reduced the expression of ANG2 and ANGPTL4 in ES-2-Luc-Ctl cells (Fig. 7b and Supplementary Fig. 5), similar to the observed effect of increased testisin. In contrast, PAR-2 loss had little effect on the low levels of ANG2 or ANGPTL4 in the testisin expressing (ES-2-Luc-TsWT) cells (Fig. 7b and Supplementary Fig. 5). These data show for the first time role for PAR-2 in the regulation of ANG2 and ANGPTL4 expression.

To further validate the role of PAR-2 in the regulation of ANG2 and ANGPTL4, PAR-2 activity was inhibited using the PAR-2 antagonist GB83 [34]. Treatment of ES-2-Luc-Ctl cells with GB83 significantly reduced ANG2 and ANGPTL4 expression, by 35% and 44% respectively (Fig. 7c). As with PAR-2 knockdown, GB83 treatment of ES-2-Luc-TsWT cells did not significantly alter the expression of either ANG2 or ANGPTL4. Together, these data demonstrate a role for PAR-2 in the regulation of ANG2 and ANGPTL4 expression and indicate that testisin inhibits ANG2 and ANGPTL4 expression by suppressing PAR-2 signaling.

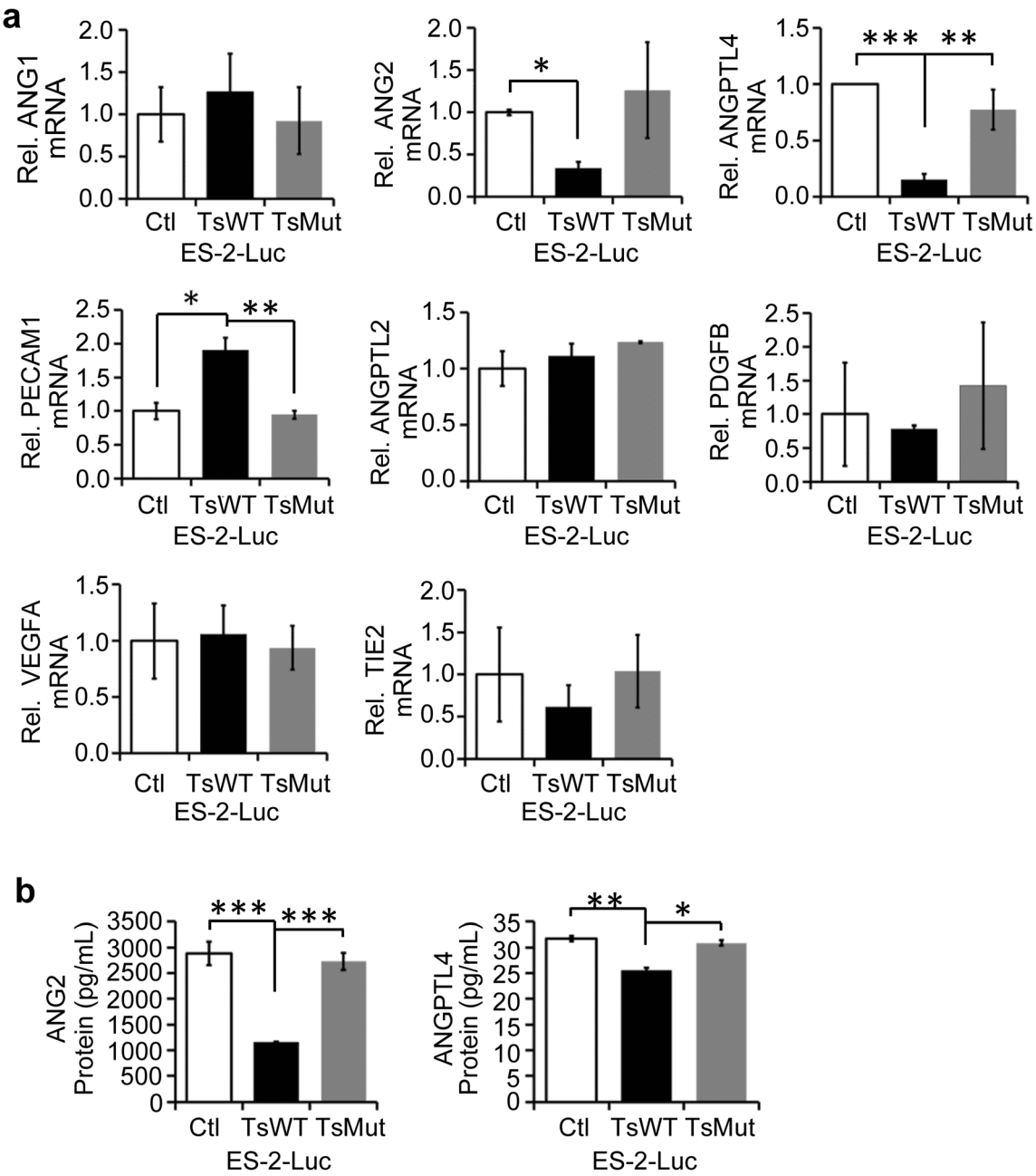

Fig. 5 Testisin proteolytic activity reduces ANG2 and ANGPTL4 gene expression in ES-2-Luc cells. qPCR validation study of genes identified to be up- or downregulated at least twofold by the TaqMan Angiogenesis Array. **a** ANG1, ANG2, ANGPTL4, PECAM1/CD31, ANGPTL2, PDGFB, VEGFA, and TIE2. mRNA expression was normalized to GAPDH and expressed relative to ES-2-Luc-Ctl cells. All graphs show mean ± SEM and are the average of at least two independent experiments from triplicate wells, $*p < 0.05$; $**p < 0.01$; $***p < 0.001$, unpaired *t* test. **b** Measurement by ELISA of ANG2 and ANGPTL4 protein levels in conditioned media collected at 24 and 48 h, respectively. Graphs show mean ± SEM and values are the average of at least two independent experiments. $*p < 0.05$; $**p < 0.01$; $***p < 0.001$, unpaired *t* test

Testisin proteolytic activity antagonizes pro-angiogenic ANG2 and ANGPTL4 during experimental ovarian tumor metastasis in vivo

To further investigate the modulation ANG2 and ANGPTL4 expression by testisin activity, the ascites fluids and tumor tissues recovered from mice bearing ES-2-Luc-TsWT, ES-2-Luc-Ctl, and ES-2-Luc-TsMut xenograft tumors were analyzed for ANG2 and ANGPTL4 expression. ELISA of clarified ascites fluid for ANG2 and ANGPTL4 protein expression showed that ascites from mice carrying ES-2-Luc-TsWT tumors contained dramatically reduced levels of both ANG2 and ANGPTL4 proteins compared to mice carrying ES-2-Luc-Ctl or ES-2-Luc-TsMut tumors (Fig. 8a). qPCR analysis of ANG2 and ANGPTL4 mRNA expression in tumor tissues scraped from the diaphragm also showed significantly reduced expression of

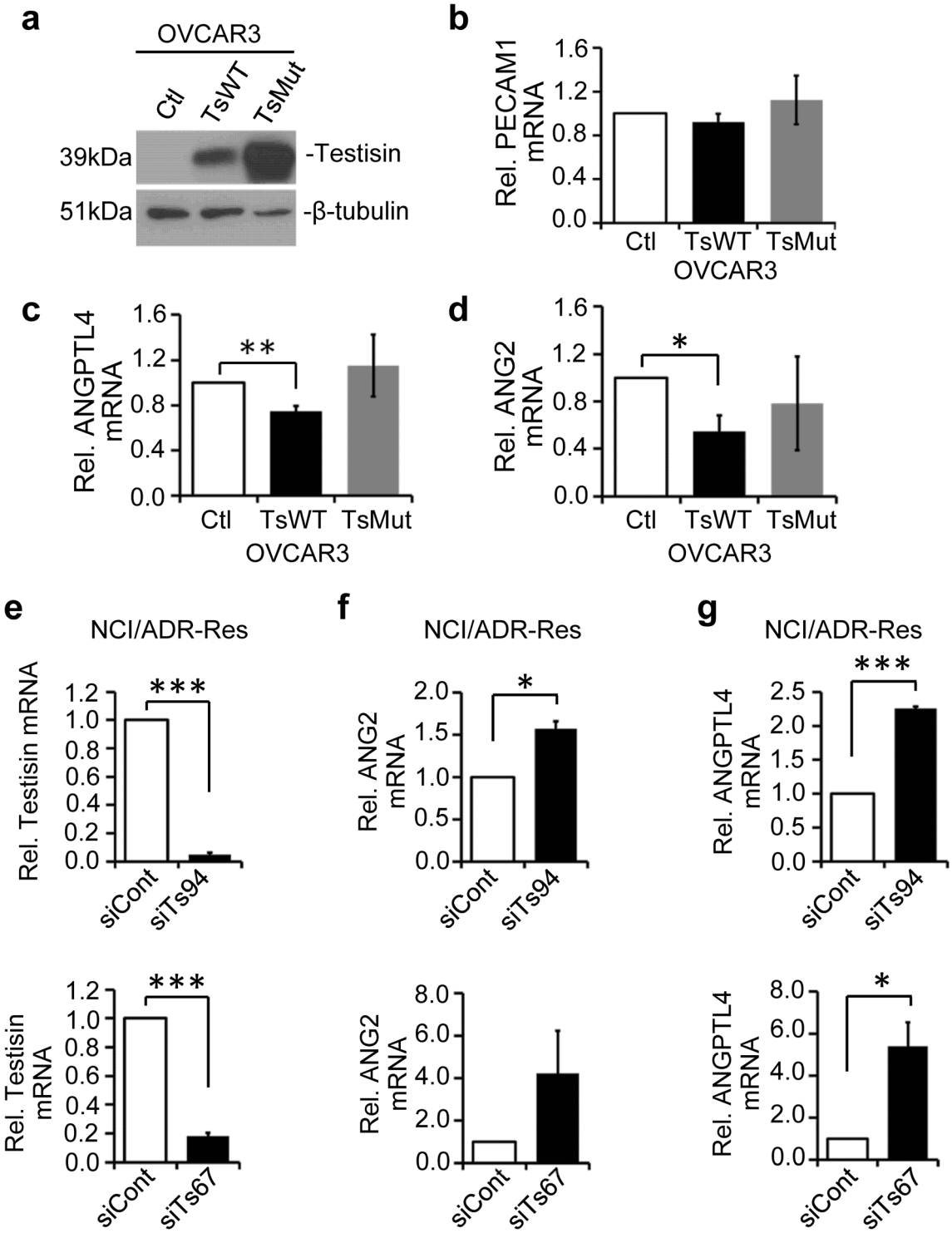

Fig. 6 Testisin activity antagonizes ANG2 and ANGPTL4 mRNA expression in ovarian cancer cells. **a** Immunoblot analysis showing significantly increased testisin protein OVCAR3-TsWT and OVCAR3-TsMut cells compared to OVCAR3-Ctl cells. **b**–**d** qPCR analysis of mRNA isolated from OVCAR3-Ctl, OVCAR3-TsWT, and OVCAR3-TsMut for PECAM1, ANGPTL4, and ANG2. mRNA expression for all genes was normalized to GAPDH and expressed relative to vector expressing cells. Graph shows mean ± SEM, and data represents the average of three independent experiments, $*p < 0.05$; $**p < 0.01$, unpaired *t* test. **e** Testisin knockdown in NCI/ADR-Res cells using two different siRNAs (siTs94 and siTs67) measured by qPCR. **f** ANG2 and **g** ANGPTL4 mRNA expression in NCI/ADR-Res cells after testisin siRNA knockdown, compared with control siRNA-treated cells. Signals were normalized to GAPDH and graphs are mean ± SEM from two independent experiments, $*p < 0.05$; $***p < 0.001$, unpaired *t* test

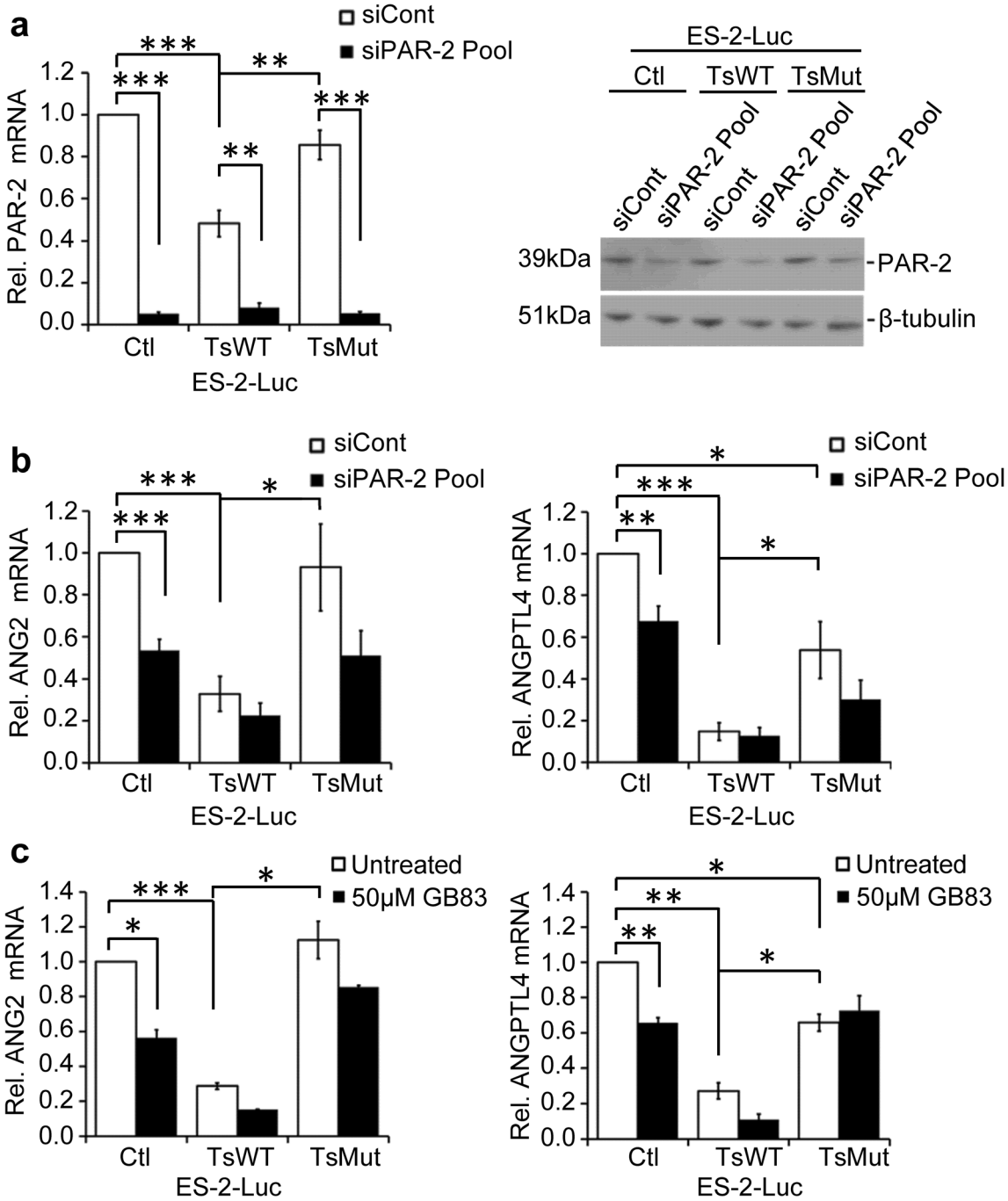

Fig. 7 PAR-2 knockdown or pharmacological inhibition antagonizes ANG2 and ANGPTL4. **a** qPCR (*left panel*) and immunoblot analysis (*right panel*) of PAR-2 expression in ES-2-Luc-Ctl, ES-2-Luc-TsWT, and ES-2-LucMut cells following PAR-2 siRNA knockdown using a siRNA pool (see also Supplementary Fig. 5). **b** ANG2 and ANGPTL4 mRNA expression in ES-2-Luc-Ctl, ES-2-Luc-TsWT, and ES-2-Luc-TsMut after PAR-2 siRNA knockdown, compared with control siRNA-treated cells. Signals were normalized to GAPDH and expressed relative to ES-2-Luc-Ctl cells. Graphs are mean ± SEM from four independent experiments, $*p < 0.05$; $**p < 0.01$; $***p < 0.001$, unpaired or one-sample *t* test. **c** qPCR analysis of ANG2 and ANGPTL4 mRNA expression after treatment with the PAR-2 antagonist, GB83 (50 μM), or vehicle alone (DMSO) for 24 h. Graphs represent the mean ± SEM from the average of two independent experiments. $*p < 0.05$; $**p < 0.01$; $***p < 0.001$, one-sample *t* test

ANG2 and ANGPTL4 mRNA transcripts in the ES-2-Luc-TsWT tumors compared to the ES-2-Luc-Ctl or ES-2-Luc-TsMut tumors, consistent with the reduced protein expression (Fig. 8b). Importantly, these in vivo data demonstrate that testisin proteolytic activity is capable of suppressing the expression and secretion of both ANG2 and ANGPTL4 in the complex environment of experimental peritoneal metastasis.

Together, these data identify a novel testisin-triggered PAR-2 pathway that results in suppression of ANG2 and ANGPTL4, important mediators of peritoneal

vascular permeability and metastatic ovarian tumor progression.

Discussion

It is critical that we understand the underlying mechanisms of ovarian cancer peritoneal metastasis to pursue more effective therapeutic strategies for chemoresistant and recurrent disease. Here, using a preclinical xenograft model of late-stage ovarian cancer metastasis, we find that testisin expression reduces ovarian metastatic tumor burden, intraperitoneal tumor colonization, and ascites formation, by a mechanism that is dependent on testisin's proteolytic activity. Moreover, we find that testisin activity antagonizes the synthesis and secretion of the pro-tumorigenic angiopoietins ANG2 and ANGPTL4 in vivo, which is likely a major contributor to the suppression of tumor metastasis in this ovarian tumor model. In vitro studies demonstrated that testisin activity causes the loss of PAR-2 from the cell surface and the suppression of PAR-2 signaling, and conversely that ANG2 and ANGPTL4 expression is dependent upon the expression and activation of PAR-2. Together, these data suggest that testisin regulation of PAR-2 induces the downregulation of these angiopoietins in this context.

Increased testisin proteolytic activity on ES-2-Luc ovarian cancer cells was found to decrease metastatic tumor dissemination and colonization of the peritoneal cavity. This finding was surprising since several hallmarks of aggressive cancer are a direct result of proteolytic activity, including tumor cell invasion into the stroma, angiogenesis, and metastasis [2], with the roles of proteases traditionally focused on protein degradation and extracellular matrix remodeling. Testisin gene expression was originally reported to be increased in advanced stage ovarian tumors [7]; however, a systematic analysis of a large gene expression microarray dataset revealed testisin to be a metastasis-associated gene that is downregulated in omental ovarian metastases compared to primary serous carcinomas [14]. This may indicate that while testisin activity promotes initial tumor dissemination, successful metastasis requires testisin downregulation at later stages, possibly via hypermethylation of a 5' CpG island in the promoter

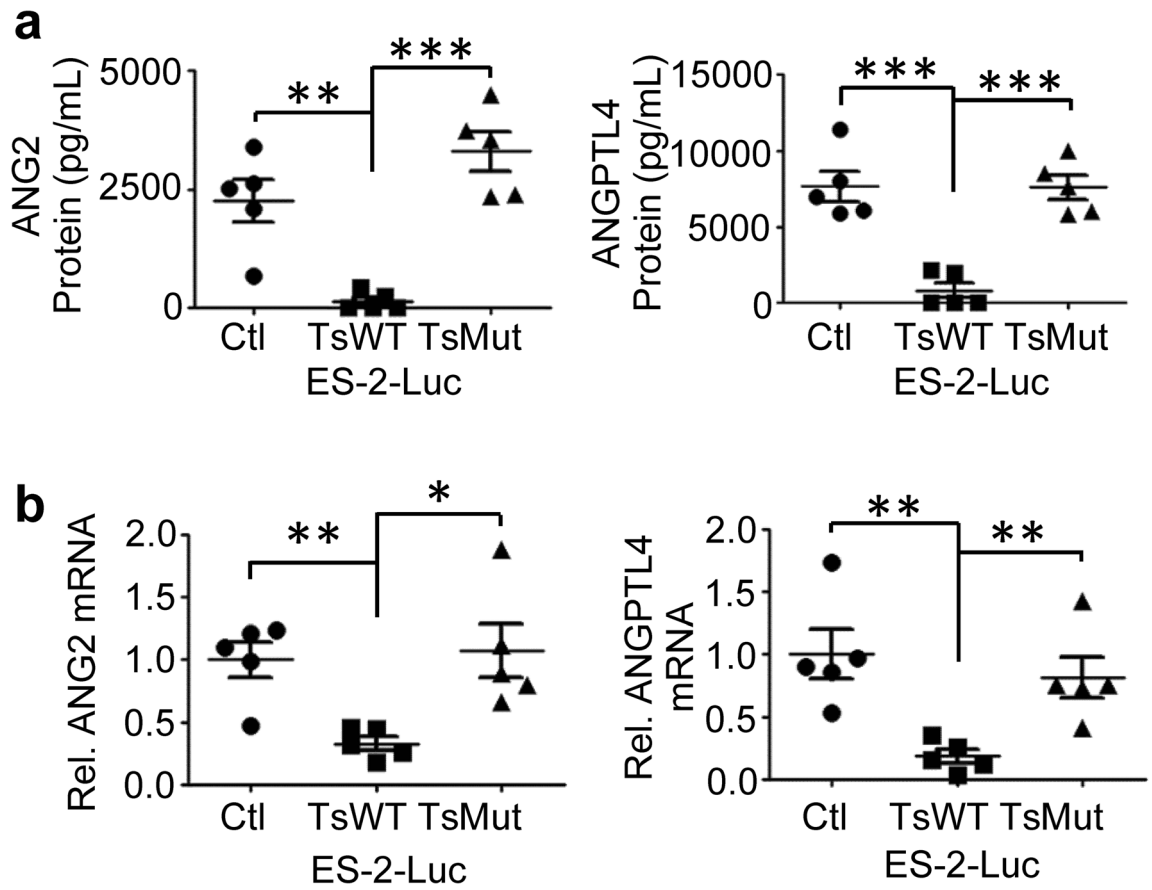

Fig. 8 Testisin proteolytic activity antagonizes ANG2 and ANGPTL4 protein expression in vivo. **a** ANG2 and ANGPTL4 protein levels in clarified ascites collected from mice as measured by ELISAs. Mean ± SEM, $n = 5$ mice per group, $^{**}p < 0.01$; $^{***}p < 0.001$, one-way ANOVA with post hoc Tukey's test. **b** ANG2 and ANGPTL4 mRNA levels in tumor tissues removed from the diaphragms of ES-2-Luc tumor-bearing mice, analyzed by qPCR. RNA expression is normalized to GAPDH. $n = 5$ mice per group. Graphs show mean ± SEM, $^{*}p < 0.05$; $^{**}p < 0.01$, one-way ANOVA with post hoc Tukey's test

region that has been shown to suppress testisin expression in testicular tumorigenesis [35]. The dampening of testisin expression at later stages of ovarian tumor metastasis could contribute to poor patient outcomes by allowing the expression of pro-tumorigenic angiopoietins promoting metastasis. In addition, our novel finding that ovarian tumor cell expressed PAR-2 is required for production of ANG2 and ANGPTL4 is consistent with the increased PAR-2 expression that is observed in human ovarian cancers, which correlates with decreased patient survival [17].

In our in vivo xenograft model of ovarian tumor metastasis, testisin proteolytic activity resulted in decreased metastatic tumor burden associated with decreased ascites formation and suppression of the synthesis and secretion of the proangiogenic factors, ANG2 and ANGPTL4. ANG2 and ANGPTL4 are both reported to be upregulated in ovarian cancers and associated with disease [36, 37]. ANG2 levels are elevated in serum collected from ovarian cancer patients and are associated with increased frequency of ascites [38]. The overexpression of ANGPTL4 in other tumors is associated with poor prognosis and poor disease-free survival rates [39]. Expression of other major modulators of vascular permeability and angiogenesis, VEGF and ANG1 [38, 40], were not significantly affected by testisin activity in our studies. ANG1 is known to induce the activation of TIE2/TEK, a surface receptor tyrosine kinase generally expressed by endothelial cells [41], and to stabilize blood vessels protecting them from VEGF-induced plasma leakage. Notably, ANG2 acts as an antagonist of the ANG1/TIE2 interaction and promotes vessel permeability and leakage that favors tumor progression. ANGPTL4 is unable to bind to the TIE2 receptor, but ANG2 and ANGPTL4 are both reported to enhance the permeability of blood vessels in murine models, inducing vascular leak and edema, by signaling to destabilize endothelial cell junctions [42–44]. As the development of ascites has been shown to be largely dependent on hyperpermeability of the peritoneal microvasculature [45], the testisin-induced suppression of ANG2 and ANGPTL4 is consistent with the reduction in ascites and reduced metastatic tumor burden observed in mice carrying ES-2-Luc-TsWT tumors.

While the angiopoietins are being investigated as potential therapeutic targets [46, 47], little is known regarding the regulation of these pro-tumorigenic factors in ovarian tumor metastasis. Our data suggest a novel pathway in which testisin-mediated proteolytic cleavage of PAR-2 suppresses their synthesis. Although mechanisms involved in the regulation of ANG2 and ANGPTL4 expression in cancer cells are poorly understood, the MAPK pathway has been implicated in other cell contexts [48, 49]. It is presently unknown whether testisin cleavage of PAR-2 in ovarian cancer cells causes PAR-2 internalization and the activation of a specific signaling pathway that suppresses ERK activation and ANG2 and ANGPTL4 gene transcription, or whether testisin is acting to remove PAR-2 from the cell surface to dampen its availability and suppress pro-tumorigenic signaling.

The targeting of ANG2 alone or in combination with drugs targeting the VEGF axis have shown therapeutic promise in cancers, including ovarian, in part through the normalization of blood vessels and the reduction of ascites in mice [46, 47, 50]. The results from our study support the targeting of ANG2 and perhaps ANGPTL4 as effective biologic therapies for reducing ovarian cancer metastases. Further, manipulation of the extracellular protease/anti-protease balance, as well as cell-type-specific inhibition or activation of PAR-2 signaling [51], may represent effective alternate or adjunct biologic therapies for metastatic ovarian cancer.

Acknowledgements We thank Eun Yong Choi, M.D., and Rena Lapidus, Ph.D., of the Translational Laboratory Shared Services, University of Maryland School of Medicine, for assistance with the in vivo tumor studies and the in vivo bioluminescence imaging.

Funding information This work was supported by the National Institutes of Health Grants R01 CA196988, R01 HL118390 and T32 CA154274.

Compliance with ethical standards

All procedures performed in studies involving animals were in accordance with the ethical standards of the University of Maryland School of Medicine Institutional Animal Care and Use Committee (IACUC), the institution at which the studies were conducted.

Conflict of interest The authors declare that they have no competing interests.

References

1. Bast RC Jr, Hennessy B, Mills GB (2009) The biology of ovarian cancer: new opportunities for translation. Nat Rev Cancer 9:415–428
2. Lengyel E (2010) Ovarian cancer development and metastasis. Am J Pathol 177:1053–1064
3. Bamias A, Pignata S, Pujade-Lauraine E (2012) Angiogenesis: a promising therapeutic target for ovarian cancer. Crit Rev Oncol Hematol 84:314–326
4. Ramakrishnan S, Subramanian IV, Yokoyama Y, Geller M (2005) Angiogenesis in normal and neoplastic ovaries. Angiogenesis 8: 169–182
5. Eskander RN, Tewari KS (2012) Emerging treatment options for management of malignant ascites in patients with ovarian cancer. Int J Women's Health 4:395–404
6. Herr D, Sallmann A, Bekes I, Konrad R, Holzheu I, Kreienberg R, Wulff C (2012) VEGF induces ascites in ovarian cancer patients via increasing peritoneal permeability by downregulation of Claudin 5. Gynecol Oncol 127:210–216
7. Shigemasa K, Underwood LJ, Beard J, Tanimoto H, Ohama K, Parmley TH, O'Brien TJ (2000) Overexpression of testisin, a serine protease expressed by testicular germ cells, in epithelial ovarian tumor cells. J Soc Gynecol Investig 7:358–362
8. Aimes RT, Zijlstra A, Hooper JD, Ogbourne SM, Sit ML, Fuchs S, Gotley DC, Quigley JP, Antalis TM (2003) Endothelial cell serine proteases expressed during vascular morphogenesis and angiogenesis. Thromb Haemost 89:561–572

9. Hooper JD, Bowen N, Marshall H, Cullen LM, Sood R, Daniels R, Stuttgen MA, Normyle JF, Higgs DR, Kastner DL, Ogbourne SM, Pera MF, Jazwinska EC, Antalis TM (2000) Localization, expression and genomic structure of the gene encoding the human serine protease testisin. Biochim Biophys Acta 1492:63–71
10. Hooper JD, Nicol DL, Dickinson JL, Eyre HJ, Scarman AL, Normyle JF, Stuttgen MA, Douglas ML, Loveland KA, Sutherland GR, Antalis TM (1999) Testisin, a new human serine proteinase expressed by premeiotic testicular germ cells and lost in testicular germ cell tumors. Cancer Res 59:3199–3205
11. Scarman AL, Hooper JD, Boucaut KJ, Sit ML, Webb GC, Normyle JF, Antalis TM (2001) Organization and chromosomal localization of the murine testisin gene encoding a serine protease temporally expressed during spermatogenesis. Eur J Biochem 268:1250–1258
12. Netzel-Arnett S, Bugge TH, Hess RA, Carnes K, Stringer BW, Scarman AL, Hooper JD, Tonks ID, Kay GF, Antalis TM (2009) The glycosylphosphatidylinositol-anchored serine protease PRSS21 (testisin) imparts murine epididymal sperm cell maturation and fertilizing ability. Biol Reprod 81:921–932
13. Tang T, Kmet M, Corral L, Vartanian S, Tobler A, Papkoff J (2005) Testisin, a glycosyl-phosphatidylinositol-linked serine protease, promotes malignant transformation *in vitro* and *in vivo*. Cancer Res 65:868–878
14. Bignotti E, Tassi RA, Calza S, Ravaggi A, Bandiera E, Rossi E, Donzelli C, Pasinetti B, Pecorelli S, Santin AD (2007) Gene expression profile of ovarian serous papillary carcinomas: identification of metastasis-associated genes. Am J Obstet Gynecol 196:245 e241–245 e211
15. Driesbaugh KH, Buzza MS, Martin EW, Conway GD, Kao JP, Antalis TM (2015) Proteolytic activation of the protease-activated receptor (PAR)-2 by the glycosylphosphatidylinositol-anchored serine protease testisin. J Biol Chem 290:3529–3541
16. Adams MN, Ramachandran R, Yau MK, Suen JY, Fairlie DP, Hollenberg MD, Hooper JD (2011) Structure, function and pathophysiology of protease activated receptors. Pharmacol Ther 130: 248–282
17. Jahan I, Fujimoto J, Alam SM, Sato E, Sakaguchi H, Tamaya T (2007) Role of protease activated receptor-2 in tumor advancement of ovarian cancers. Ann Oncol 18:1506–1512
18. Ruf W, Yokota N, Schaffner F (2010) Tissue factor in cancer progression and angiogenesis. Thromb Res 125(Suppl 2):S36–S38
19. Chanakira A, Westmark PR, Ong IM, Sheehan JP (2017) Tissue factor-factor VIIa complex triggers protease activated receptor 2-dependent growth factor release and migration in ovarian cancer. Gynecol Oncol 145:167–175
20. Luo R, Wang X, Dong Y, Wang L, Tian C (2014) Activation of protease-activated receptor 2 reduces glioblastoma cell apoptosis. J Biomed Sci 21:25
21. Iablokov V, Hirota CL, Peplowski MA, Ramachandran R, Mihara K, Hollenberg MD, MacNaughton WK (2014) Proteinase-activated receptor 2 (PAR2) decreases apoptosis in colonic epithelial cells. J Biol Chem 289:34366–34377
22. Huang SH, Li Y, Chen HG, Rong J, Ye S (2013) Activation of proteinase-activated receptor 2 prevents apoptosis of lung cancer cells. Cancer Investig 31:578–581
23. Aman M, Ohishi Y, Imamura H, Shinozaki T, Yasutake N, Kato K, Oda Y (2017) Expression of protease-activated receptor-2 (PAR-2) is related to advanced clinical stage and adverse prognosis in ovarian clear cell carcinoma. Hum Pathol 64:156–163
24. Schaffner F, Yokota N, Ruf W (2012) Tissue factor proangiogenic signaling in cancer progression. Thromb Res 129(Suppl 1):S127–S131
25. Zhu T, Sennlaub F, Beauchamp MH, Fan L, Joyal JS, Checchin D, Nim S, Lachapelle P, Sirinyan M, Hou X, Bossolasco M, Rivard GE, Heveker N, Chemtob S (2006) Proangiogenic effects of protease-activated receptor 2 are tumor necrosis factor-alpha and consecutively Tie2 dependent. Arterioscler Thromb Vasc Biol 26: 744–750
26. Shaw TJ, Senterman MK, Dawson K, Crane CA, Vanderhyden BC (2004) Characterization of intraperitoneal, orthotopic, and metastatic xenograft models of human ovarian cancer. Mol Ther 10:1032–1042
27. Rothmeier AS, Ruf W (2012) Protease-activated receptor 2 signaling in inflammation. Semin Immunopathol 34:133–149
28. Johnson JJ, Miller DL, Jiang R, Liu Y, Shi Z, Tarwater L, Williams R, Balsara R, Sauter ER, Stack MS (2016) Protease-activated Receptor-2 (PAR-2)-mediated Nf-kappaB activation suppresses inflammation-associated tumor suppressor microRNAs in oral squamous cell carcinoma. J Biol Chem 291:6936–6945
29. Wang Y, Xu RC, Zhang XL, Niu XL, Qu Y, Li LZ, Meng XY (2012) Interleukin-8 secretion by ovarian cancer cells increases anchorage-independent growth, proliferation, angiogenic potential, adhesion and invasion. Cytokine 59:145–155
30. Lane D, Matte I, Rancourt C, Piche A (2011) Prognostic significance of IL-6 and IL-8 ascites levels in ovarian cancer patients. BMC Cancer 11:210
31. Tanaka Y, Sekiguchi F, Hong H, Kawabata A (2008) PAR2 triggers IL-8 release via MEK/ERK and PI3-kinase/Akt pathways in GI epithelial cells. Biochem Biophys Res Commun 377:622–626
32. Shi J, Wei PK (2016) Interleukin-8: a potent promoter of angiogenesis in gastric cancer. Oncol Lett 11:1043–1050
33. Ning Y, Manegold PC, Hong YK, Zhang W, Pohl A, Lurje G, Winder T, Yang D, LaBonte MJ, Wilson PM et al (2011) Interleukin-8 is associated with proliferation, migration, angiogenesis and chemosensitivity *in vitro* and *in vivo* in colon cancer cell line models. Int J Cancer 128:2038–2049
34. Barry GD, Suen JY, Le GT, Cotterell A, Reid RC, Fairlie DP (2010) Novel agonists and antagonists for human protease activated receptor 2. J Med Chem 53:7428–7440
35. Manton KJ, Douglas ML, Netzel-Arnett S, Fitzpatrick DR, Nicol DL, Boyd AW, Clements JA, Antalis TM (2005) Hypermethylation of the 5' CpG island of the gene encoding the serine protease testisin promotes its loss in testicular tumorigenesis. Br J Cancer 92:760–769
36. Hata K, Udagawa J, Fujiwaki R, Nakayama K, Otani H, Miyazaki K (2002) Expression of angiopoietin-1, angiopoietin-2, and Tie2 genes in normal ovary with corpus luteum and in ovarian cancer. Oncology 62:340–348
37. Zhu P, Tan MJ, Huang RL, Tan CK, Chong HC, Pal M, Lam CR, Boukamp P, Pan JY, Tan SH et al (2011) Angiopoietin-like 4 protein elevates the prosurvival intracellular O2(-):H2O2 ratio and confers anoikis resistance to tumors. Cancer Cell 19:401–415
38. Sallinen H, Heikura T, Laidinen S, Kosma VM, Heinonen S, Yla-Herttuala S, Anttila M (2010) Preoperative angiopoietin-2 serum levels: a marker of malignant potential in ovarian neoplasms and poor prognosis in epithelial ovarian cancer. Int J Gynecol Cancer 20:1498–1505
39. Tan MJ, Teo Z, Sng MK, Zhu P, Tan NS (2012) Emerging roles of angiopoietin-like 4 in human cancer. Mol Cancer Res 10:677–688
40. Santin AD, Hermonat PL, Ravaggi A, Cannon MJ, Pecorelli S, Parham GP (1999) Secretion of vascular endothelial growth factor in ovarian cancer. Eur J Gynaecol Oncol 20:177–181
41. Fagiani E, Christofori G (2013) Angiopoietins in angiogenesis. Cancer Lett 328:18–26
42. Huang RL, Teo Z, Chong HC, Zhu P, Tan MJ, Tan CK, Lam CR, Sng MK, Leong DT, Tan SM et al (2011) ANGPTL4 modulates vascular junction integrity by integrin signaling and disruption of intercellular VE-cadherin and claudin-5 clusters. Blood 118:3990–4002
43. Hakanpaa L, Sipila T, Leppanen VM, Gautam P, Nurmi H, Jacquemet G, Eklund L, Ivaska J, Alitalo K, Saharinen P (2015)

Endothelial destabilization by angiopoietin-2 via integrin beta1 activation. Nat Commun 6:5962

44. Roviezzo F, Tsigkos S, Kotanidou A, Bucci M, Brancaleone V, Cirino G, Papapetropoulos A (2005) Angiopoietin-2 causes inflammation in vivo by promoting vascular leakage. J Pharmacol Exp Ther 314:738–744
45. Nagy JA, Herzberg KT, Dvorak JM, Dvorak HF (1993) Pathogenesis of malignant ascites formation: initiating events that lead to fluid accumulation. Cancer Res 53:2631–2643
46. Papadopoulos KP, Kelley RK, Tolcher AW, Razak AR, Van Loon K, Patnaik A, Bedard PL, Alfaro AA, Beeram M, Adriaens L et al (2016) A phase I first-in-human study of nesvacumab (REGN910), a fully human anti-angiopoietin-2 (Ang2) monoclonal antibody, in patients with advanced solid tumors. Clin Cancer Res 22:1348–1355
47. Mazzieri R, Pucci F, Moi D, Zonari E, Ranghetti A, Berti A, Politi LS, Gentner B, Brown JL, Naldini L, de Palma M (2011) Targeting the ANG2/TIE2 axis inhibits tumor growth and metastasis by impairing angiogenesis and disabling rebounds of proangiogenic myeloid cells. Cancer Cell 19:512–526
48. Liu N, Cui C, Sun Y, Zhang F, Wang S, Su G, Cai X (2017) Hydrogen peroxide promotes the expression of angiopoietin like 4 in RAW264.7 macrophages via MAPK pathways. Mol Med Rep 16:6128–6133
49. Niu G, Carter WB (2007) Human epidermal growth factor receptor 2 regulates angiopoietin-2 expression in breast cancer via AKT and mitogen-activated protein kinase pathways. Cancer Res 67:1487–1493
50. Tuppurainen L, Sallinen H, Karvonen A, Valkonen E, Laakso H, Liimatainen T, Hytonen E, Hamalainen K, Kosma VM, Anttila M et al (2017) Combined gene therapy using AdsVEGFR2 and AdsTie2 with chemotherapy reduces the growth of human ovarian cancer and formation of ascites in mice. Int J Gynecol Cancer 27:879–886
51. Hamilton JR, Trejo J (2017) Challenges and opportunities in protease-activated receptor drug development. Annu Rev Pharmacol Toxicol 57:349–373